HHS Public Access

Author manuscript

Bone. Author manuscript; available in PMC 2021 January 01.

Published in final edited form as:

Bone. 2020 January ; 130: 115126. doi:10.1016/j.bone.2019.115126.

The Age-Related Decrease in Material Properties of BALB/c Mouse Long Bones Involves Alterations to the Extracellular Matrix

Amy Creecy, PhD[1,2,3], **Sasidhar Uppuganti, MS**[2,3], **Madeline R. Girard, BS**[1], **Siegfried G. Schlunk, BS**[1], **Chidi Amah, BS**[4], **Mathilde Granke, PhD**[2,3], **Mustafa Unal, PhD**[2,3,5], **Mark D. Does, PhD**[1], **Jeffry S. Nyman, PhD**[1,2,3,6,*]

[1]Department of Biomedical Engineering, Vanderbilt University, Nashville, TN 37232

[2]Department of Orthopaedic Surgery & Rehabilitation, Vanderbilt University Medical Center, Nashville, TN 37232

[3]Center for Bone Biology, Vanderbilt University Medical Center, Nashville, TN 37232

[4]Meharry Medical College, Nashville, TN 37208

[5]Department of Mechanical Engineering, Karamanoglu Mehmetbey University, Karaman, Turkey 70100

[6]Department of Veterans Affairs, Tennessee Valley Healthcare System, Nashville, TN 37212

Abstract

One possibility for the disproportionate increase in fracture risk with aging relative to the decrease in bone mass is an accumulation of changes to the bone matrix which deleteriously affect fracture resistance. In order to effectively develop new targets for osteoporosis, a preclinical model of the age-related loss in fracture resistance needs to be established beyond known age-related decreases in bone mineral density and bone volume fraction. To that end, we examined long bones of male and female BALB/c mice at 6-mo. and 20-mo. of age and assessed whether material and matrix properties of cortical bone significantly differed between the age groups. The second moment of area of the diaphysis (minimum and maximum principals for femur and radius, respectively) as measured by ex vivo micro-computed tomography (μCT) was higher at 20-mo. than at 6-mo. for

[*]**Correspondence**: Jeffry S. Nyman, Vanderbilt Orthopaedic Institute, 1215 21st Ave S, Suite 4200, Nashville, TN 37232, jeffry.s.nyman@vumc.org, o: (615) 936-6296.

Acknowledgment of Contributors

Study Design: JSN conceived the study with advice from AC, MG, and MDD. Study Conduct: AC, SU, MRG, SGS, CA, MG, and MU primarily conducted the experiments. Data analysis: AC, SU, MRG, SGS, CA, MG, and MU contributed to the acquisition of data and the analysis of the data. These authors worked with JSN to ensure the accuracy and integrity of the results. Data interpretation: All authors provided interpretation of various results. Drafting manuscript: AC and JSN with input from all co-authors wrote the draft of the manuscript. Revising manuscript content: JSN, SU, MU, MG, and MDD helped AC revise the manuscript. Approving final version of manuscript: AC, SU, MRG, SGS, CA, MG, MU, MDD, and JSN approve the final content in the present paper. JSN takes responsibility for the integrity of the data analysis.

Supplemental Data is included with this manuscript.

both males and females, but ultimate moment as measured by three-point bending tests did not decrease with age. Cortical thickness was lower with age for males, but higher for old females. Partially accounting for differences in structure, material estimates of yield, ultimate stress, and toughness (left femur) were 12.6%, 11.1%, and 40.9% lower, respectively, with age for both sexes. The ability of the cortical bone to resist crack growth (right femur) was also 18.1% less for the old than for the young adult mice. These decreases in material properties were not due to changes in intracortical porosity as pore number decreased with age. Rather, age-related alterations in the matrix were observed for both sexes: enzymatic and non-enzymatic crosslinks by high performance liquid chromatography increased (femur), volume fraction of bound water by ^{1}H-nuclear magnetic resonance relaxometry decreased (femur), cortical tissue mineral density by μCT increased (femur and radius), and an Amide I sub-peak ratio I_{1670}/I_{1640} by Raman spectroscopy increased (tibia). Overall, there are multiple matrix changes to potentially target that could prevent the age-related decrease in fracture resistance observed in BALB/c mouse.

Keywords

bone quality; toughness; bound water; advanced glycation end-products; collagen; Raman spectroscopy

1. Introduction

With aging, there are deleterious changes to bone at multiple hierarchical levels of organization that lower the overall fracture resistance and hence elevate fracture risk. As examples, the cortices become thinner (macrostructure) causing less bone area for resisting axial forces [1–3]; intracortical porosity [4–6] and fenestrations in trabeculae increase (microstructure) [7] while the volume of trabecular bone decreases [8,9] such that the apparent strength is reduced [10], as predicted by finite element analysis [11–14]; and advanced glycation end-products (AGEs) accumulate [15–17] within the organic matrix (ultrastructure) of cortical bone impeding the deformation of collagen fibrils [18]. Traditionally, osteoporosis is viewed as a problem of low bone mass causing reduced bone strength, but during aging, there is a well-known disproportionate increase in fracture risk relative to the decrease in areal bone mineral density (aBMD) [19,20]. Therefore, in addition to reducing fracture risk by minimizing the propensity to fall, improving muscle strength and flexibility, and maintaining nutrition among the elderly, there is a need to identify mechanisms that can be targeted to promote bone quality, not just bone mass or volume.

To date, the primary concern in pre-clinical rodent studies has been whether a therapy increases bone mass and bone strength, typically aBMD or bone volume fraction (BV/TV) and structural-dependent strength (e.g., maximum force in compression or ultimate moment during bending), even though mechanical testing studies of cadaveric bone from adult donors report age-related declines in material properties (percent *decline* per decade): ultimate tensile strength [21] (~2.1% [22]), impact energy (~8.4% [23]), energy-to-failure in tension (6.8% [22]), work-of-fracture in bending (~8.7% [24]), fatigue resistance (~23% [25]), and fracture toughness (~4.1% [24] or ~6.8% [26]), all determined at the apparent level (i.e., independent of macrostructure but not microstructure). The focus on whole-bone

strength is understandable given that mice and rats experience a decrease in trabecular BV/TV at metaphyseal sites of the femur and tibia [27–34] as well as within the lumbar vertebral body [28,35,36] with advanced aging (>20-mo. vs. 6-mo. or 12-mo.). Moreover, similar to humans [1,37,38], cortical thickness in long bones of C567BL/6J mice [27,39] and Fischer F344 rats [33] is known to decrease without an accompanying loss in cortical area or second moment of area of the mid-shaft due to periosteal expansion with age.

While several studies report that the estimated yield or ultimate stress of cortical bone, as determined by three-point bending tests of femur mid-shaft, decreases with advanced aging (i.e., beyond 12-mo.) for C57BL/6 mice [39–41], little is known about the age-related changes in the material properties of bone for the BALB/c mouse strain, another pre-clinical model of aging supported by the National Institute on Aging (NIA) in the US. In a study of long bones from female and male BALB/c mice at 2-, 4-, 7-, 12-, 20-months (mo.) of age, the yield stress and ultimate stress was found to not significantly change with aging after skeletal maturity (7-mo. vs. 20-mo.) when the radius was tested in three-point bending [32]. Although the femur mid-shaft was also loaded-to-failure in three-point bending, these estimates of bending strength at the material level were not reported for this region of cortical bone [32]. Whether the ability to dissipate energy during failure (toughness) and resist crack growth (fracture toughness), two other important material properties that characterize fracture resistance of bone, decrease with advanced aging in C57BL/6 or BALB/c mice is not known at present for both sexes.

While the quality of the bone matrix is thought to decline after middle age [15] and presumably contributes to the increase in fracture risk due to osteoporosis and other diseases of bone [42], potential therapeutics for reducing fracture risk are primarily assessed for their ability to prevent or rescue bone loss in rodent models of sex hormone deficiency [43]. While such an approach is understandable, it may not fully assess the efficacy of the therapeutic. For example, sodium fluoride treatment was tested in clinical trials for the treatment of osteoporosis because pre-clinical studies found that it increased bone mass [44], but this therapy did not reduce fracture risk despite increasing aBMD because fluoride gets incorporated into the mineral, thereby lowering the mechanical integrity of bone [45]. When mechanical testing was included, the energy-at-failure and strain-at-failure of the femur mid-shaft was lower for the rats treated with NaF compared to sham and ovariectomized rats without this treatment [46]. There are also mouse models of disease such as osteogenesis imperfecta in which the mineral-to-matrix ratio and bone mineral density are higher while the ultimate stress and toughness of the cortical bone is lower for the mice with the disease (e.g., collagen defect) than for the control mice [47]. If new therapeutic strategies are to target the contribution of bone matrix quality to fracture resistance, a well-validated, preclinical model in which age-related changes in the matrix accompany a loss in multiple material properties, not just strength, would be useful [48]. In particular, the objective of this study was to identify the matrix properties of cortical bone that change with advanced aging in a mouse strain for which aging colonies are maintained by commercial laboratories with support from the NIA. Previous studies characterizing the bone matrix of mice have been limited to skeletal development (1 to 40 days of age) [49] or to male C57BL/6 mice (6-mo., 18-mo., 24-mo.) [41]. We hypothesized that the age-related decrease in fracture resistance is similar between humans and BALB/c mice in that i) the ability of bone to dissipate energy

and resist crack growth is lower for both male and female, 20-month-old BALB/c mice compared to young-adult (6-month-old), sex-matched BALB/c mice and ii) such changes coincide with age-related changes within the bone matrix (e.g., higher AGEs, higher type B carbonate substitutions, and lower bound water).

2. Materials and Methods

2.1. Study design and tissue collection

Forty male BALB/c mice at 19 months (n=20) or 2 months of age (n=20) were first acquired from the colony maintained by the NIA (Charles River Laboratories), and then several years later 40 female BALB/c mice at 19 months (n=20) or 4–5 months of age (n=20) were acquired from the same colony. All procedures were approved by the Vanderbilt University Medical Center IACUC. Mice were housed with no more than 5 mice per cage on a 12-hour light/dark cycle. Mice were fed a standard rodent chow (5L0D, LabDiet, St Louis, MO) ad libitum and were euthanized by cervical dislocation after cardiac exsanguination to collect blood serum while under deep anesthesia at 6 months (6-mo.) and 20 months (20-mo.). These 2 age groups were chosen to represent young adulthood after skeletal maturation and post-senescence [50], with the awareness that median lifespan of BALB/c mice is ~100 days less than the median lifespan of C57BL/6 mice [51]. Two old mice per sex died soon after arriving and were not included in the study, and so bones were available from twenty 6-mo. old mice per sex and eighteen 20-mo. old mice per sex.

Femurs were immersed in phosphate buffered saline (PBS) and stored at −20 °C. Right femurs were subsequently notched at the mid-point of the diaphysis for later use in fracture toughness testing. This involved mounting the femur to a micrometer stage such that the axial length of the bone was perpendicular to a diamond-embedded, circular wafering blade (Buehler Isomet 3×0.007”) and then translating the mid-shaft a set distance ($1/5^{th}$ anterior-posterior width) into the irrigated blade as it rotated. Then the notch was sharpened using a razorblade coated in diamond solution (representative images of the notch with a micro-notch shown in Figure S1). Tibiae and radii were flash frozen in liquid nitrogen and stored at −80 °C.

2.2. Micro-computed tomography analysis

The notched region of each right femur (1.86 mm in length) was imaged using a μCT50 scanner (Scanco Medical AG, Brüttisellen, Switzerland) and the following scan parameters: X-ray tube voltage of 70 kVp drawing 114 μA, an isotropic voxel size of 6 μm, and an acquisition of 1000 projections per 360° rotation with an integration time of 600 ms. The mid-point (1.26 mm in length) of the left femur diaphysis was imaged using a μCT40 scanner (Scanco Medical AG, Brüttisellen, Switzerland): X-ray tube voltage of 70 kVp drawing 114 μA, an isotropic voxel size of 12 μm, and an acquisition of 1000 projections per 360° rotation with an integration time of 300 ms. The central point of curvature (1.09 mm in length) of each radius was imaged using a μCT50: X-ray tube voltage of 55 kVp drawing 200 μA, an isotropic voxel size of 4 μm, and an acquisition of 1000 projections per 360° rotation with an integration time of 1500 ms. For each scanner, a 0.5 mm Al filter was used along with the manufacturer’s specified beam hardening correction for the corresponding

hydroxyapatite (HA) phantom calibration, which is performed weekly on both scanners. The global threshold for each scan protocol (4 μm, 6 μm, and 12 μm voxel sizes) was selected to minimize the contribution of noise and maximize the inclusion of bone tissue (Figure S2).

Following reconstruction, the notch angle was manually determined as previously described [52]. Upon fitting tight contours to the periosteal surface for slices above and below the notch, we used standard Scanco evaluation scripts to determine tissue mineral density of the cortex (Ct.TMD) and cortical porosity (Ct.Po) at 6 μm for a global threshold of >960.9 mgHA/cm^3 (Gaussian image noise filter: sigma = 0.2 and support = 2) (representative histograms shown in Figure S2) and a global, inverse threshold of <1021.3 mgHA/cm^3 (sigma = 0.3 and support = 1) (representative pore images shown in Figure S3), respectively. To determine the cross-sectional geometry parameters, cortical thickness (Ct.Th) and Ct.TMD of the mid-shafts at 12 μm (femur) and at 4 μm (radius), we also used standard Scanco evaluation scripts (IPLV6_AUTOCONTOUR_DUALTH_GAUSS_SLIMIRR.COM and IPLV6_MIDSHAFT.COM) with the following parameters: i) a sigma=0.2, support=1, and global threshold of >666.8 mgHA/cm^3 (right radius) and ii) sigma=0.2, support=1 and global threshold of >751.4 mgHA/cm^3 (left femur). The Ct.Po of the intact left femur was also determined for a global inverse threshold of <900.4 mgHA/cm^3 (sigma = 0.2 and support = 1).

2.3. Assessing material properties of cortical bone

Hydrated left femurs and right radii were loaded-to-failure at 3 mm/min in three-point bending using a servo-hydraulic material testing system (Instron DynaMight 8841, Norwood, MA) with a 100 N load cell (Honeywell, OH, Model no. 060-C863–02). For each bone, the anterior side faced down (tension), while the medial side faced forward. The lower span for the bending tests of the femurs was adjusted to approximately maintain a span-to-anterior-posterior-width ratio of 6.0 (varied between 6 mm and 8 mm in increments of 0.5 mm). The intact radii were all tested using a constant span of 8 mm. Force and displacement data was collected and used to calculate structural-dependent ultimate moment (ultimate or maximum force × span / 4) and rigidity (stiffness, or slope of the linear portion of the data, × span^3 / 48). Material properties were estimated using the cross-sectional geometry parameters from μCT. The second moment of area for bending in the anterior-posterior (a-p) direction and about the medial-lateral axis corresponds to the minimum principal or I_{min} of the femur and the maximum principal or I_{max} of the radius, and the distance between the neutral axis and the periosteal surface in direction of loading corresponds to the length of the minimum principal axis (c_{min}) of the femur (Table S5) or the maximum principal axis (c_{max}) of the radius as previously described [33].

To slowly propagate a crack, notched right femurs were loaded in three-point bending under hydration at 0.5 mm/min until failure [53]. The posterior side face downward, and the span was adjusted to be 4 times the anterior-posterior width rounded to the nearest 0.1 mm. Stable crack propagation was monitored using a high resolution DSLR camera (Canon EOS 7D) attached with a macro lens. To determine the fracture toughness of cortical bone, the critical stress intensity factor to initiate crack growth ($K_{c,init}$) was calculated from yield force and a previously published equation for mode I opening of a circumferential flaw in a cylindrical

pipe [53]. As described in our previous publication [52], notch angle and bone geometry parameters were determined from the μCT evaluations and met the criteria that makes the equation valid [53]. Similar to the toughness estimate for the intact femur, the energy dissipated during crack propagation was estimated as the work-to-failure during crack growth (W_{crack}) normalized to the cortical area (Ct.Ar) and adjusted for span as previously described [33].

2.4. Raman spectroscopy

Raman spectra were collected from 10 sites randomly distributed within the mid-shaft of the left tibiae (Figure S4A) for males and the right tibiae for females using an 830 nm confocal Raman micro-spectroscopy (Invia, Renishaw, Hoffman Estates, IL), providing ~1 cm^{-1} spectral resolution. Unfortunately, the right tibia from male mice was not available for Raman analysis, but we verified that there were no bias in the left-right measurements of the Raman properties for the female bones (Figure S5). An average of 10 consecutive spectra (Figure S4B) were collected per site with a 20X objective (NA=0.40) for a 5 s duration. Laser power was set at ~ 35 mW. Spectra were processed as previously described [54,55]. Briefly, the 10 raw Raman spectra per bone specimen were averaged to maximize signal-to-noise (Figure S4C) [56]. Then, background fluorescence was removed from all averaged spectra by subtracting a 5^{th}-order polynomial function from the base of the raw spectra (Figure S4D). Next, the averaged spectra were further smoothed to minimize noise (Figure S4E) using a proprietary de-noising (D-n) algorithm provided by the LabSpec 5 software (v5.78.24, Horiba Jobin Yvon, Edison, NJ). From the averaged and de-noised spectrum per bone sample, we calculated the following Raman peak ratios: ν_1PO_4/Amide I, ν_1PO_4/Proline, ν_1PO_4/Amide III, ν_1PO_4/CH_2-wag, and CO_3/ν_1PO_4. Crystallinity was the inverse of the line-width of the ν_1PO_4 peak at half the height from baseline or half-maximum (1/FWHM). To assess potential age-related differences in the secondary structure of collagen I, Amide I sub-peak ratios were calculated directly from the intensity ratios of the Amide I peak per sub-peak, the location of which was identified from the local minima of each second-derivative spectrum (Intensity at approximate wavenumber location): I_{1670}/I_{1640}, I_{1670}/I_{1610}, and I_{1670}/I_{1690} [56].

2.5 ^{1}H nuclear magnetic resonance (^{1}H NMR) relaxometry

Bound water and pore water were measured using our published ^{1}H NMR relaxometry technique [33,57] on the intact right femurs prior to notching and fracture toughness tests. After removing any surface water by a dry Kim-wipe, the bone was placed within a custom, low-proton radiofrequency (RF) coil along with a reference marker of water (20 μL). After placing the coil in a 4.7 T horizontal-bore magnet (Varian Medical Systems, Santa Clara, CA), Carr-Purcell-Meiboom-Gill (CPMG) measurements with a total of 10,000 echoes were acquired at an echo spacing of 100 μs. Each T2 spectrum (Figure S6) was generated by fitting multiple exponential decay functions to the measurements, and the integrated area of bound water signal was converted to volume (based on a reference marker of known volume of water) and normalized to bone volume as measured using Archimedes' principle. To estimate the pore water volume, we integrated the peaks between 0.61 ms and 46 ms excluding long T2's that overlap signals from lipids (Figure S6). Bound water signals were integrated between 0.1 ms and 0.61 ms.

2.6. High Performance Liquid Chromatography (HPLC)

The proximal and distal ends of the left femur were removed and the remaining cortical bone was flushed prior to complete demineralization in 20% ethylene diamine tetra-acetic acid (EDTA) at 4°C. Bones were subsequently dehydrated and then hydrolyzed in 6 N HCl with 4.5 mM alpha-amino-N-butyric acid (α-ABA) for 20 hours at 100 °C. Hydrolysates were filtered and split into approximately ~1 mg fractions. One fraction was used to measure the crosslinks pyridinoline (PYD), deoxypyridinoline (DPD), and pentosidine (PE) on a C-18 Spherisorb ODS2 column (Waters, Milford, MA) using a reverse-phase HPLC protocol previously described [58].

A second ~1 mg hydrolysate fraction was used to measure hydroxyproline. Hydrolysates were derivatized using phenoisothiocyanate (PITC) and measured on a PicoTag® column (Waters, Milford, MA) using a previously described protocol [58]. Hydroxyproline values were calculated from a standard curve normalizing to α-ABA. Crosslink values were normalized to a collagen content value estimated from hydroxyproline.

2.7. Statistical Analysis

Since the female and male mice were not siblings, age comparisons were made separately. Due to some variables not passing Shapiro-Wilk test for normality (Table S1), the Mann-Whitney test was used to determine whether properties were significantly different between the age groups (GraphPad Prism v6, GraphPad Software, La Jolla, CA). To investigate whether age-related changes were different between the sexes, we tested whether age group, sex, and the interaction between the two factors significantly explained the variance in each property (Table S2) using bootstrapped general linear models (GLMs) with 500 replications in STATA (StataCorp LLC., College Station, TX) in which age and sex were categorical variables (Table S2).

3. Results

3.1. The Diaphysis of Long Bones of Older Mice Had Higher Bone Area But Similar Structural-dependent Strength Compared to Younger Mice

Though there was no difference in body weight between the young and old female mice (Table 1), the minimum principal second moment of area or area moment of inertia (I_{min}), was higher at 20-mo. than at 6-mo. for both the femur and radius diaphysis (Figure 1B–D). For males, body weight was significantly lower at 20-mo. compared to 6-mo. (Table 1), but as with females, I_{min} was higher at 20-mo. (Figure 1B–D) for both bones. Additional structural differences in the mid-shaft included higher Ct.Ar (female only) and higher Tt.Ar with aging (Table 1). Interestingly, while cortical thickness (Ct.Th) was higher in older female mice, it was lower in 20-mo. old male mice compared to respective young adult mice (Figure 1E–F). In best-fit general linear models (GLMs), these relative differences in I_{min} and Ct.Th (femur and radius) between the age groups were significant when body mass was included as a covariate, regardless of sex (Table S3).

Matching the age-related increase in I_{min}, the yield and ultimate moment of the femur diaphysis was also higher in old females compared to young-adult females (Table 1). In

contrast, there were no differences in these structural-dependent terms between 20-mo. and 6-mo. for males, even though I_{min} was higher for the older mice (Table 1). As for the radius, yield and ultimate moment was higher at 20-mo. than at 6-mo. for both females and males (Table 1). Again, in best-fit GLMs, yield and ultimate moment of the radius (female and male) and yield and ultimate moment of the femur (female only) were significantly higher with age when body mass was included as covariate (Table S3).

Cortical porosity can also influence bending strength at the apparent level, but for the intact femur mid-shaft (central region), which was scanned at a 12 μm voxel size (Figure 2A), cortical porosity (Ct.Po) was barely detectable, and so no age-related differences were observed (Figure 2C). For the right femur scanned at a 6 μm voxel size (Figure 2B), evaluated above and below the notch (but still the central region), the female BALB/c mice had lower Ct.Po at 20-mo. than at 6-mo. (Figure 2D). Interestingly, both females and males had fewer pores at 20-mo. compared to 6-mo. in both femurs (Figure 2E–F). In concordance with the lack of an age-related increase in cortical porosity, the volume fraction of pore water, as determined by ^{1}H NMR, was lower for the 20-mo. than for the 6-mo. old bones, irrespective of sex (Tables S1 and S2). Thus, in BALB/c mice, there was not an age-related increase in cortical porosity that could counteract the age-related increase in the structural resistance to bending (section modulus or I_{min}/c_{min}).

3.2. The Cortical Bone of Old Mice Dissipated Less Energy (toughness) with Less Resistance to Crack Growth (fracture toughness) Compared to Young Adult Mice

When comparing estimated material properties of cortical bone at the femur diaphysis, yield stress (Figure 3C) and ultimate stress (Tables S1 and S3) was indeed lower at 20-mo. compared to 6-mo. for male and female BALB/c mice. However, for the diaphysis of the radius, there were no age-related differences in yield stress and ultimate stress (Figure 3D, Tables S1 and S2). The toughness of cortical bone was also lower at 20-mo. compared to 6-mo. (Figure 3E). As one exception though, toughness did not differ between young-adult and aged mice when the female radii were tested in three-point bending (Figure 3F). Post-yield toughness (PY Tough.) and post-yield displacement (PYD) followed the same trends as toughness with cortical bone becoming more brittle with age (Table 1). In fracture toughness tests on the right femur (Figures 4A and 4B), the stress intensity to initiate crack growth, $K_{c,init}$, was lower at 20-mo. for both females and males (Figure 4C). Similarly, the work done during crack growth normalized to cortical area (W_{crack}/Ct.Ar) was lower at 20-mo. compared to 6-mo. for female and male BALB/c mice (Figure 4D).

3.4. Compositional Properties of the Bone Matrix Changed with Age in Both Female and Male BALB/c Mice

There were multiple age-related changes within the matrix. Ct.TMD of the intact femur mid-shaft (12 μm) and notched femur mid-shaft (6 μm) was higher at 20-mo. compared to 6-mo. in both sexes (Figures 5A and 5B, respectively). Similarly, mineral-to-matrix ratios (MMRs) of the tibia midshaft were all higher at 20-mo. (Table 2). With respect to the mineral phase of the matrix, both Type B carbonate and crystallinity was higher with advanced age (Table 2). Multiple Amide I sub-peak ratios related to the secondary structure of collagen I significantly differed between the age groups. Both I_{1670}/I_{1610} and I_{1670}/I_{1640} were higher

for 20-mo. than for 6-mo., irrespective of sex (Table 2). Interestingly, the so-called matrix maturity ratio I_{1670}/I_{1690} did not significantly differ with age for females but was significantly lower at 20-mo. that at 6-mo. for males (Table 2). The mature enzymatic crosslink PYD, as measured by HPLC was higher at 20-mo. than at 6-mo. (Figure 5C). Similarly, PE, a non-enzymatic crosslink, was higher in 20-mo. mice for both female and male BALB/c mice (Figure 5E), though the peak of this crosslink as well as deoxypyridinoline (DPD) was quite small in the chromatograms (Figure S7). Lastly, the volume fraction of bound water, as measured by ^{1}H-NMR was lower at 20-mo. compared to 6-mo. for both sexes (Figure 5D).

4. Discussion

With advanced aging, the femurs of BALB/c mice became brittle having less ability to dissipate energy during fracture and less ability to resist crack growth, regardless of sex. Thus, in addition to the age-related loss in trabecular BV/TV or aBMD, the BALB/c model of aging includes a similar deterioration in the material properties of cortical bone as observed in human bone. Notably, the whole-bone strength measurements, yield and ultimate moment endured by diaphysis during bending, were either not different (femurs from males) between the age groups or higher at 20-mo. than at 6mo., even when adjusting for the influence of body mass on bone size (Table S3). Accompanying the deterioration in fracture resistance are a number of changes within the bone matrix: an increase in tissue mineral density, an increase in amount of carbonate in the mineral lattice, alterations in the secondary structure of type 1 collagen (Amide I sub-peak ratios), an increase in enzymatic crosslinks (mature hyroxylysyl-pyridinoline) and a non-enzymatic crosslink (pentosidine), and a decrease in matrix-bound water. Except for the increase in TMD, all these changes occur in the cortical bone of humans with aging. As such, the BALB/c strain can perhaps serve as a pre-clinical model of age-related changes in bone matrix fragility in addition to a model of age-related decrease in bone mass.

While this is the first study to show that energy dissipated during bending to failure and resistance to crack growth of mouse bone is lower at 20-mo. than at 6-mo. for both male and female BALB/c mice, previous work by Willinghamm et al. characterized changes in bone through skeletal maturity (2-mo., 4-mo., and 7-mo.) and with aging (7-mo., 12-mo., and 20-mo.) [32]. Consistent with this previous study, we also observed for both sexes higher Ct.TMD and higher I_{min} at 20-mo. compared to young adult mice (Figure 1 and Figure 5). As for the radius, both studies found that Ct.TMD and moment of inertia were higher for old than for young adult BALB/c mice, regardless of sex. Likewise, yield stress of the radius mid-shaft did not vary between 6-mo. or 7-mo. and 20-mo in both studies of the aging phenotype of BALB/c cortical bone. We confirmed that the previously observed age-related trend in decreasing post-yield displacement of the diaphysis (femur and radius) among male BALB/c mice [32] is significant. As for female BALB/c mice, both studies found that deflection after yielding (Py-d) was significantly lower at 20-mo. than at 6–7-mo. for the femur diaphysis (Figure S8) but not for the radius diaphysis (Figure S9). The effect size of each reported property is available in the supplemental materials (Table S1) and can be used to determine either the minimum number of animals needed for a desired type I error probability (α) and type II error probability (β) or the post-hoc power for a given number of

animals and α. Fewer than 18 mice per group appear sufficient to determine differences in multiple bone properties between the 2 age groups given the calculated effect sizes (Table S1).

There were few notable differences in the age-related changes in bone between male and female, non-sibling, BALB/c mice (Table S2). While body mass was lower in males at 20-mo. than at 6-mo., it did not significantly decrease with aging for females. Cortical thickness was lower in males at 20-mo. compared to 6 mo., but it was higher in females with advanced age (Figure 1). Based on the Willinghamm et al. study [32], cortical thickness for females appears to peak at 12-mo. as opposed to 7-mo., which could be one reason for this apparent sex-related discrepancy. Age-related changes in cross-sectional properties were also not the same between sexes. For example, cortical area (Ct.Ar) of the femur mid-shaft was only higher at 20-mo. than at 6-mo. for the female mice (Figure 5F and Table 1). As indicated by the GLMs (Table S3), Ct.Th of the femur mid-shaft positively depended on age and body mass of the females only suggesting the age-related increase in Ct.Ar is partially due to the weight gain. Also, compared to 6-mo., yield moment and ultimate moment of the femur midshaft were ~30% greater with age, whereas there were no differences between the age groups for the male mice. Again, in the linear regression models, the ultimate moment depended on age and body mass of females (Table S3), but not on age or body mass of males. Moreover, the section modulus (I_{min}/c_{min} or $I_{a\text{-}p}/c_{a\text{-}p}$) of female mid-shafts explained 43% and 66% of the variance in yield moment and ultimate moment, respectively; whereas the section modulus of male mid-shafts only explained 13% and 19% of the variance in these bending strength measurements of the femur mid-shaft, respectively (Table S4). Thus, this sex-related discrepancy in strength gain with age is partially due to an apparent weight gain occurring only in the female mice. Age-related changes in matrix properties (tissue mineral density, mineral-to-matrix ratio, structure of mineral and organic phase, pyridinoline) were however consistent between males and females (Table S2), while bound water and pentosidine had a greater change with age for male than for the female mice (significant interaction in Table S3, Figures 5D and 5E).

There are of course limitations to the use of mice in studying cortical bone, namely the lack of extensive osteonal remodeling throughout the lifespan and hence the lack of cement lines as a microstructural barrier to fracture. Nonetheless, in this study, similarities between age-related deficits in human bone and mouse bone were observed. Specifically, between 6-mo. and 20-mo. of age, BALB/c mice showed a greater or similar age-related decrease in post-yield toughness (59% for female and 48% male on average) and in crack initiation toughness (13% for female and 23% for male on average) than the age-related decrease in yield stress (13% for both female and male on average). Unlike human and mouse bone, $K_{c,init}$ of cortical bone (femur mid-shaft) increased with age in Fischer F344 male rats, another NIA-supported colony. Like humans, rats typically experience an increase in cortical porosity at the mid-shaft near the endosteum [33], while Ct.Po of the mid-shaft does not vary with age in mice (Figure 2) unless assessed at the distal and proximal ends of the diaphysis [36]. Thus, when testing the femur mid-shaft in three-point bending, BALB/c mice phenocopy the decrease in material properties of cortical bone but not the increase in cortical porosity with aging; whereas F344 rats phenocopy the increase in cortical porosity and the decrease in

yield stress and in post-yield toughness with aging but not the age-related decrease in crack initiation toughness.

There were multiple changes to the matrix that may lower the fracture resistance of bone. While in general material properties such as toughness are thought to be influenced by the organic matrix, degree of mineralization (ash fraction) is known to be inversely proportional to impact energy as observed from the mechanical testing of bones from different species with a wide range in the degree of mineralization [59]. Thus, the age-related increase in Ct.TMD could have conferred lower toughness in the old mice. However, at odds with the paradigm of material strength being directly proportional to TMD or bone density [60], yield stress (Figure 3) and ultimate stress (Tables S2 and S3) was lower for the old mice than for the young adult mice or not different (radius). In addition, Ct.TMD did not significantly help section modulus predict the yield moment of either the femur or radius (Table S4). Also, apparent modulus of either long bone did not differ between the age groups. This suggests other matrix-related factors are influencing the material properties. For example, bound water has been observed to decrease with age in humans, and it correlates with fracture toughness [26] and ultimate strength [57] of human cortical bone. The age-related decrease in bound water (Figure 5) could potentially reduce plasticity of the bone while also lowering material strength since hydration confers flexibility to collagen I and transfers loads between organic matrix and mineral phase.

Other observed changes in the matrix likely also influence the age-related decrease in material properties. Multiple sub-peak ratios in the Amide I band were different between the age groups. Particularly, the ratio I_{1670}/I_{1640} was higher with age (Table 2). This sub-peak ratio negatively correlates with toughness of bovine cortical bone [55] and the fracture toughness of human cortical bone [61]. Thermal denaturation, which lowers bone toughness, increased this sub-peak ratio [62,63]. The so-called matrix maturity ratio (I_{1670}/I_{1690}) was lower for old than for the young adult male mice, but did not significantly change between old and young adult female mice. Given that both mature enzymatic crosslinks and non-enzymatic crosslinks were higher with age (Figure 5), irrespective of sex, our direct measurement of I_{1670}/I_{1690} is not likely an indicator of an age-related difference in the collagen crosslinking profile. Also, glycated bone in glucose or ribose to induce AGE accumulation decreases I_{1670}/I_{1640} [56], and so another age-related mechanism likely affects the structure of type 1 collagen. Broadly, Amide I sub-peak ratios are indicators of the secondary structure of collagen I [64], which can be affected radiolysis of collagen I [64], enzymatic crosslinking [65], and fatigue damage [62]. Thus, the higher sub-peak ratios I_{1670}/I_{1610} and I_{1670}/I_{1640} (i.e., loss of helical order) with age could indicate an embrittling effect. Also, since bound water exists because of hydrogen bonding with the hydrophilic residues of collagen I and electrostatic attractions to the surfaces of mineral crystals, increases in mineralization could displace bound water from the matrix [66]. In effect, the age-related loss in material properties is likely multifactorial with regards to matrix properties.

The present study did not include multiple age groups, very high-resolution techniques to measure small pores (e.g., lacunae by light microscopy, scanning electron microscopy, synchrotron μCT), and other analytical techniques for characterization the matrix (e.g.,

nanoindentation, Fourier-transform infrared spectroscopy, X-ray diffraction). Thus, additional work is necessary i) to identify at what age, toughness or fracture toughness peaks and then declines in male and female BALB/c mice, ii) to establish whether lacunar volume or distribution of small pores changes with age, and iii) to identify the biomechanical mechanism(s) that describes the decrease in fracture toughness of mouse bone with respect to lamellar heterogeneity, collagen fibril mechanics, and interactions between the organic matrix and the mineral phase of bone. Nonetheless, the present work shows that the ability of cortical bone to resist crack growth decreases with age in the pre-clinical BALB/c model of aging, and this decrease accompanies changes in the matrix. Moreover, it hints at potential targets related to post-translation modifications affecting collagen structure and bound water.

There are limitations to the mechanical testing of long bones from rodents that perhaps partially explain the observed age-related differences in mechanical properties between the radius and femur. The equations for estimating material properties were derived assuming the cross-sections of the diaphyseal cortex are uniform, axisymmetric and remain perpendicular to the deflection curve when the bone is loaded, assuming the bone behaves as an isotropic, linear elastic material, and assuming the transverse strain is negligible (i.e., the flexural stress and strain are dominant). For three-point bending tests of non-uniform, mouse long bones, the determination of yield stress depends on i) the consistent placement of the mid-shaft such that the orientation (anterior down & medial forward) matches I_{min}/c_{min} (a deviation of 5° from the principal axes causes an error of 1.9% or less in the yield stress calculation; Table S5) or I_{max}/c_{max} and ii) the span relative to the anterior-posterior (a-p) width of the bone (i.e., aspect ratio) in the direction of loading ($c_{a\text{-}p}$). In effect, the slenderer mouse radius experiences less shear stress or transverse strain than the less slender mouse femur [67]. As such, the estimated yield stress of the femur appeared to be lower than the yield stress of the radius when they are likely similar. While we adjusted the span to match the a-p width of the femur in an attempt to normalize the aspect ratio, age-related differences in the estimated material strength are not entirely independent of the age-related increases in the second area of moment (Table S6, negative association between yield stress and section modulus, $I_{a\text{-}p}/c_{a\text{-}p}$). The age-related decrease in the estimated toughness measurements was independent of cross-sectional bone geometry. Given the curvature of the radius relative to the straighter femur mid-shaft, its material properties are estimated by three-point bending as well, but the dependence of material strength on section modulus is less pronounced compared to the femur (Table S6). The age-related decrease in yield or ultimate stress and in toughness primarily occurring when the femur was tested suggests that age-related changes in the matrix are affecting the ability of cortical bone to resist shear deformation.

As seen in this study with BALB/c mice, the age-related loss in fracture resistance may be the result of multiple changes to the matrix. Thus, the efficacy of therapeutics that target bone matrix quality either through targeting AGE formation, matrix hydration, or collagen structure can be tested in aging BALB/c model (male and female). As examples, an AGE-inhibitor such as pyridoxamine, could potentially improve material properties assuming AGE accumulation contributes to the age-related loss in fracture toughness [68]. Similarly, raloxifene could improve bone toughness of old mice by increasing matrix hydration [69]. Drugs that target the health of osteocytes is another possible way to improve material

properties as there is emerging evidence that osteocytes regulate mineralization and possibly proteins in the peri-lacunar matrix [70]. There are multiple mechanisms by which the bone matrix can be manipulated to possibly improve fracture resistance using BALB/c mice.

5. Conclusions

Strength, toughness, and fracture toughness at the material level are lower at 20-mo. than at 6-mo. for the BALB/c model of aging. This loss of fracture resistance may be the result of the multiple changes to cortical bone at the matrix level. While it is unclear which matrix-level change facilitates the loss of fracture resistance with aging, female and male BALB/c mouse is a suitable pre-clinical model of aging for the development of therapeutics that target the matrix.

Supplementary Material

Refer to Web version on PubMed Central for supplementary material.

Acknowledgements

This work was funded in part by a training grant from NIDDK (DK101003) and by grants from the National Institute of Arthritis and Musculoskeletal and Skin Diseases (AR067871) and the Department of Veterans Affairs (VA), Veterans Health Administration, Office of Research and Development (BX004297). The use of the micro-computed tomography scanner (μCT50) was made possible by a National Institutes of Health (NIH) grant (S10RR027631-01). The content provided herein does not necessarily reflect the views of NIH or VA.

Grant Supporters: NIDDK, NIAMS, VA

References

[1]. Macdonald HM, Nishiyama KK, Kang J, Hanley DA, Boyd SK, Age-related patterns of trabecular and cortical bone loss differ between sexes and skeletal sites: a population-based HR-pQCT study, J. Bone Miner. Res 26 (2011) 50–62. doi:10.1002/jbmr.171. [PubMed: 20593413]

[2]. Milovanovic P, Adamu U, Simon MJK, Rolvien T, Djuric M, Amling M, et al., Age- and Sex-Specific Bone Structure Patterns Portend Bone Fragility in Radii and Tibiae in Relation to Osteodensitometry: A High-Resolution Peripheral Quantitative Computed Tomography Study in 385 Individuals, J Gerontol a-Biol. 70 (2015) 1269–1275. doi:10.1093/gerona/glv052.

[3]. Kral R, Osima M, Borgen TT, Vestgaard R, Richardsen E, Bjørnerem Å, Increased cortical porosity and reduced cortical thickness of the proximal femur are associated with nonvertebral fracture independent of Fracture Risk Assessment Tool and Garvan estimates in postmenopausal women, PLoS ONE. 12 (2017) e0185363–15. doi:10.1371/journal.pone.0185363. [PubMed: 28945789]

[4]. Nirody JA, Cheng KP, Parrish RM, Burghardt AJ, Majumdar S, Link TM, et al., Spatial distribution of intracortical porosity varies across age and sex, Bone. 75 (2015) 88–95. doi: 10.1016/j.bone.2015.02.006. [PubMed: 25701139]

[5]. Sundh D, Nilsson AG, Nilsson M, Johansson L, Mellstrom D, Lorentzon M, Increased cortical porosity in women with hip fracture, J. Intern. Med 281 (2017) 496–506. doi:10.1111/joim. 12587. [PubMed: 28097725]

[6]. Andreasen CM, Delaisse J-M, van der Eerden BCJ, van Leeuwen JPTM, Ding M, Andersen TL, Understanding Age-Induced Cortical Porosity in Women: The Accumulation and Coalescence of Eroded Cavities Upon Existing Intracortical Canals Is the Main Contributor, J. Bone Miner. Res 33 (2018) 606–620. doi:10.1002/jbmr.3354. [PubMed: 29193312]

[7]. Fields AJ, Keaveny TM, Trabecular architecture and vertebral fragility in osteoporosis, Curr Osteoporos Rep. 10 (2012) 132–140. doi:10.1007/s11914-012-0097-0. [PubMed: 22492119]

[8]. Thomsen JS, Niklassen AS, Ebbesen EN, Brüel A, Age-related changes of vertical and horizontal lumbar vertebral trabecular 3D bone microstructure is different in women and men, 57 (2013) 47–55. doi:10.1016/j.bone.2013.07.025.

[9]. Chen H, Zhou X, Shoumura S, Emura S, Bunai Y, Age- and gender-dependent changes in three-dimensional microstructure of cortical and trabecular bone at the human femoral neck, Osteoporos Int. 21 (2009) 627–636. doi:10.1007/s00198-009-0993-z. [PubMed: 19543764]

[10]. Perilli E, Baleani M, Ohman C, Fognani R, Baruffaldi F, Viceconti M, Dependence of mechanical compressive strength on local variations in microarchitecture in cancellous bone of proximal human femur, J Biomech. 41 (2008) 438–446. doi:10.1016/j.jbiomech.2007.08.003. [PubMed: 17949726]

[11]. Mueller TL, Christen D, Sandercott S, Boyd SK, van Rietbergen B, Eckstein F, et al., Computational finite element bone mechanics accurately predicts mechanical competence in the human radius of an elderly population, 48 (2011) 1232–1238. doi:10.1016/j.bone.2011.02.022.

[12]. Easley SK, Chang MT, Shindich D, Hernandez CJ, Keaveny TM, Biomechanical effects of simulated resorption cavities in cancellous bone across a wide range of bone volume fractions, J. Bone Miner. Res 27 (2012) 1927–1935. doi:10.1002/jbmr.1657. [PubMed: 22576976]

[13]. Vilayphiou N, Boutroy S, Sornay-Rendu E, van Rietbergen B, Chapurlat R, Age-related changes in bone strength from HR-pQCT derived microarchitectural parameters with an emphasis on the role of cortical porosity, Bone. 83 (2016) 233–240. doi:10.1016/j.bone.2015.10.012. [PubMed: 26525593]

[14]. Musy SN, Maquer G, Panyasantisuk J, Wandel J, Zysset PK, Not only stiffness, but also yield strength of the trabecular structure determined by non-linear μFE is best predicted by bone volume fraction and fabric tensor, J Mech Behav Biomed Mater. 65 (2017) 808–813. doi: 10.1016/j.jmbbm.2016.10.004. [PubMed: 27788473]

[15]. Wang X, Shen X, Li X, Agrawal CM, Age-related changes in the collagen network and toughness of bone, 31 (2002) 1–7. [PubMed: 12110404]

[16]. Nyman JS, Roy A, Tyler JH, Acuna RL, Gayle HJ, Wang X, Age-related factors affecting the postyield energy dissipation of human cortical bone, 25 (2007) 646–655. doi:10.1002/jor.20337.

[17]. Odetti P, ROSSI S, Monacelli F, POGGI A, CIRNIGLIARO M, FEDERICI M, et al., Advanced glycation end products and bone loss during aging, Ann. N. Y. Acad. Sci 1043 (2005) 710–717. doi:10.1196/annals.1333.082. [PubMed: 16037297]

[18]. Zimmermann EA, Schaible E, Bale H, Barth HD, Tang SY, Reichert P, et al., Age-related changes in the plasticity and toughness of human cortical bone at multiple length scales, Proc Natl Acad Sci U S A. 108 (2011) 14416–14421. doi:10.1073/pnas.1107966108. [PubMed: 21873221]

[19]. Kanis JA, Johnell O, Oden A, Dawson A, De Laet C, Jonsson B, Ten year probabilities of osteoporotic fractures according to BMD and diagnostic thresholds, Osteoporos Int. 12 (2001) 989–995. [PubMed: 11846333]

[20]. Siris ES, Brenneman SK, Barrett-Connor E, Miller PD, Sajjan S, Berger ML, et al., The effect of age and bone mineral density on the absolute, excess, and relative risk of fracture in postmenopausal women aged 50–99: results from the National Osteoporosis Risk Assessment (NORA), Osteoporos Int. 17 (2006) 565–574. doi:10.1007/s00198-005-0027-4. [PubMed: 16392027]

[21]. McCalden RW, McGeough JA, Barker MB, Court-Brown CM, Age-related changes in the tensile properties of cortical bone. The relative importance of changes in porosity, mineralization, and microstructure, J Bone Joint Surg Am. 75 (1993) 1193–1205. [PubMed: 8354678]

[22]. Burstein AH, Reilly DT, Martens M, Aging of bone tissue: mechanical properties, J Bone Joint Surg Am. 58 (1976) 82–86. [PubMed: 1249116]

[23]. Currey JD, Brear K, Zioupos P, The effects of ageing and changes in mineral content in degrading the toughness of human femora, J Biomech. 29 (1996) 257–260. [PubMed: 8849821]

[24]. Zioupos P, Currey JD, Hamer AJ, The role of collagen in the declining mechanical properties of aging human cortical bone, J Biomed Mater Res. 45 (1999) 108–116. [PubMed: 10397964]

[25]. Diab T, Sit S, Kim D, Rho J, Vashishth D, Age-dependent fatigue behaviour of human cortical bone, Eur J Morphol. 42 (2005) 53–59. doi:10.1080/09243860500095539. [PubMed: 16123024]

[26]. Granke M, Makowski AJ, Uppuganti S, Does MD, Nyman JS, Identifying Novel Clinical Surrogates to Assess Human Bone Fracture Toughness, J Bone Miner Res. 30 (2015) 1290–1300. doi:10.1002/jbmr.2452. [PubMed: 25639628]

[27]. Halloran BP, Ferguson VL, Simske SJ, Burghardt A, Venton LL, Majumdar S, Changes in bone structure and mass with advancing age in the male C57BL/6J mouse, J. Bone Miner. Res 17 (2002) 1044–1050. doi:10.1359/jbmr.2002.17.6.1044. [PubMed: 12054159]

[28]. Glatt V, Canalis E, Stadmeyer L, Bouxsein ML, Age-related changes in trabecular architecture differ in female and male C57BL/6J mice, 22 (2007) 1197–1207. doi:10.1359/jbmr.070507.

[29]. Pietschmann P, Skalicky M, Kneissel M, Rauner M, Hofbauer G, Stupphann D, et al., Bone structure and metabolism in a rodent model of male senile osteoporosis, Exg. 42 (2007) 1099–1108. doi:10.1016/j.exger.2007.08.008.

[30]. Buie HR, Moore CP, Boyd SK, Postpubertal Architectural Developmental Patterns Differ Between the L3 Vertebra and Proximal Tibia in Three Inbred Strains of Mice, J. Bone Miner. Res 23 (2008) 2048–2059. doi:10.1359/jbmr.080808. [PubMed: 18684086]

[31]. Duque G, Rivas D, Li W, Li A, Henderson JE, Ferland G, et al., Age-related bone loss in the LOU/c rat model of healthy ageing, Exp Gerontol. 44 (2009) 183–189. doi:10.1016/j.exger.2008.10.004. [PubMed: 18992316]

[32]. Willinghamm MD, Brodt MD, Lee KL, Stephens AL, Ye J, Silva MJ, Age-related changes in bone structure and strength in female and male BALB/c mice, 86 (2010) 470–483. doi:10.1007/s00223-010-9359-y.

[33]. Uppuganti S, Granke M, Makowski AJ, Does MD, Nyman JS, Age-related changes in the fracture resistance of male Fischer F344 rat bone, Bone. 83 (2016) 220–232. doi:10.1016/j.bone.2015.11.009. [PubMed: 26610688]

[34]. Perrien DS, Akel NS, Dupont-Versteegden EE, Skinner RA, Siegel ER, Suva LJ, et al., Aging alters the skeletal response to disuse in the rat, Am. J. Physiol. Regul. Integr. Comp. Physiol 292 (2007) R988–96. doi:10.1152/ajpregu.00302.2006. [PubMed: 17068163]

[35]. Ke HZ, Qi H, Chidsey-Frink KL, Crawford DT, Thompson DD, Lasofoxifene (CP-336,156) protects against the age-related changes in bone mass, bone strength, and total serum cholesterol in intact aged male rats, 16 (2001) 765–773. doi:10.1359/jbmr.2001.16.4.765.

[36]. Ucer S, Iyer S, Kim H-N, Han L, Rutlen C, Allison K, et al., The Effects of Aging and Sex Steroid Deficiency on the Murine Skeleton Are Independent and Mechanistically Distinct, J. Bone Miner. Res 32 (2016) 560–574. doi:10.1002/jbmr.3014. [PubMed: 27714847]

[37]. Riggs BL, Melton LJ, Robb RA, Camp JJ, Atkinson EJ, Peterson JM, et al., Population Based Study of Age and Sex Differences in Bone Volumetric Density, Size, Geometry, and Structure at Different Skeletal Sites, J. Bone Miner. Res 19 (2004) 1945–1954. doi:10.1359/jbmr.040916. [PubMed: 15537436]

[38]. Silva MJ, Jepsen KJ, Age-Related Changes in Whole-Bone Structure and Strength, in: Skeletal Aging and Osteoporosis, Springer, Berlin, Heidelberg, Berlin, Heidelberg, 2012: pp. 1–30. doi:10.1007/8415_2012_137.

[39]. Ferguson VL, Ayers RA, Bateman TA, Simske SJ, Bone development and age-related bone loss in male C57BL/6J mice, 33 (2003) 387–398. doi:10.1016/S8756-3282(03)00199-6.

[40]. Almeida M, Han L, Martin-Millan M, Plotkin LI, Stewart SA, Roberson PK, et al., Skeletal involution by age-associated oxidative stress and its acceleration by loss of sex steroids, J Biol Chem. 282 (2007) 27285–27297. doi:10.1074/jbc.M702810200. [PubMed: 17623659]

[41]. Heveran CM, Schurman CA, Acevedo C, Livingston EW, Howe D, Schaible EG, et al., Chronic kidney disease and aging differentially diminish bone material and microarchitecture in C57Bl/6 mice, Bone. 127 (2019) 91–103. doi:10.1016/j.bone.2019.04.019. [PubMed: 31055118]

[42]. Bala Y, Seeman E, Bone's Material Constituents and their Contribution to Bone Strength in Health, Disease, and Treatment, (2015) 1–19. doi:10.1007/s00223-015-9971-y.

[43]. Rachner TD, Khosla S, Hofbauer LC, Osteoporosis: now and the future, Lancet. 377 (2011) 1276–1287. doi:10.1016/S0140-6736(10)62349-5. [PubMed: 21450337]

[44]. Modrowski D, Miravet L, Feuga M, Bannié F, Marie PJ, Effect of fluoride on bone and bone cells in ovariectomized rats, J. Bone Miner. Res 7 (1992) 961–969. doi:10.1002/jbmr.5650070813. [PubMed: 1442210]

[45]. Fratzl P, Roschger P, Eschberger J, Abendroth B, Klaushofer K, Abnormal bone mineralization after fluoride treatment in osteoporosis: a small-angle x-ray-scattering study, J. Bone Miner. Res 9 (1994) 1541–1549. doi:10.1002/jbmr.5650091006. [PubMed: 7817799]

[46]. Giavaresi G, Fini M, Gnudi S, Mongiorgi R, Ripamonti C, Zati A, et al., The mechanical properties of fluoride-treated bone in the ovariectomized rat, Calcif Tissue Int. 65 (1999) 237–241. doi:10.1007/s002239900690. [PubMed: 10441658]

[47]. Daley E, Streeten EA, Sorkin JD, Kuznetsova N, Shapses SA, Carleton SM, et al., Variable bone fragility associated with an Amish COL1A2 variant and a knock-in mouse model, J Bone Miner Res. 25 (2010) 247–261. doi:10.1359/jbmr.090720. [PubMed: 19594296]

[48]. Hernandez CJ, van der Meulen MC, Understanding Bone Strength Is Not Enough, J Bone Miner Res. 34 (2017) 195. doi:10.1002/jbmr.3078.

[49]. Miller LM, Little W, Schirmer A, Sheik F, Busa B, Judex S, Accretion of bone quantity and quality in the developing mouse skeleton, 22 (2007) 1037–1045. doi:10.1359/jbmr.070402.

[50]. Dutta S, Sengupta P, Men and mice: Relating their ages, Life Sci. 152 (2016) 244–248. doi:10.1016/j.lfs.2015.10.025. [PubMed: 26596563]

[51]. Yuan R, Tsaih S-W, Petkova SB, Marin de Evsikova C, Xing S, Marion MA, et al., Aging in inbred strains of mice: study design and interim report on median lifespans and circulating IGF1 levels, Aging Cell. 8 (2009) 277–287. doi:10.1111/j.1474-9726.2009.00478.x. [PubMed: 19627267]

[52]. Makowski AJ, Uppuganti S, Wadeer SA, Whitehead JM, Rowland BJ, Granke M, et al., The loss of activating transcription factor 4 (ATF4) reduces bone toughness and fracture toughness, 62 (2014) 1–9. doi:10.1016/j.bone.2014.01.021.

[53]. Ritchie RO, Koester KJ, Ionova S, Yao W, Lane NE, Ager III JW, Measurement of the toughness of bone: A tutorial with special reference to small animal studies, 43 (2008) 798–812. doi:10.1016/j.bone.2008.04.027.

[54]. Creecy A, Uppuganti S, Unal M, Clay Bunn R, Voziyan P, Nyman JS, Low bone toughness in the TallyHO model of juvenile type 2 diabetes does not worsen with age, Bone. 110 (2018) 204–214. doi:10.1016/j.bone.2018.02.005. [PubMed: 29438824]

[55]. Unal M, Jung H, Akkus O, Novel Raman Spectroscopic Biomarkers Indicate That Postyield Damage Denatures Bone's Collagen, J Bone Miner Res. 31 (2016) 1015–1025. doi:10.1002/jbmr.2768. [PubMed: 26678707]

[56]. Unal M, Uppuganti S, Leverant CJ, Creecy A, Granke M, Voziyan P, et al., Assessing Glycation-mediated Changes in Human Cortical Bone with Raman Spectroscopy, J Biophotonics. 11 (2018) e201700352. doi:10.1002/jbio.201700352. [PubMed: 29575566]

[57]. Horch RA, Gochberg DF, Nyman JS, Does MD, Non-invasive Predictors of Human Cortical Bone Mechanical Properties: T2-Discriminated 1H NMR Compared with High Resolution X-ray, PLoS ONE. 6 (2011) e16359. doi:10.1371/journal.pone.0016359. [PubMed: 21283693]

[58]. Creecy A, Uppuganti S, Merkel AR, O'Neal D, Makowski AJ, Granke M, et al., Changes in the Fracture Resistance of Bone with the Progression of Type 2 Diabetes in the ZDSD Rat, 99 (2016) 289–301. doi:10.1007/s00223-016-0149-z.

[59]. Currey JD, Effects of differences in mineralization on the mechanical properties of bone, Philos. Trans. R. Soc. Lond., B, Biol. Sci 304 (1984) 509–518. [PubMed: 6142490]

[60]. Unal M, Creecy A, Nyman JS, The Role of Matrix Composition in the Mechanical Behavior of Bone, Curr Osteoporos Rep. 16 (2018) 205–215. doi:10.1007/s11914-018-0433-0. [PubMed: 29611037]

[61]. Unal M, Uppuganti S, Timur S, Mahadevan-Jansen A, Akkus O, Nyman JS, Assessing matrix quality by Raman spectroscopy helps predict fracture toughness of human cortical bone, Sci Rep. 9 (2019) 7195–13. doi:10.1038/s41598-019-43542-7. [PubMed: 31076574]

[62]. Flanagan CD, Unal M, Akkus O, Rimnac CM, Raman spectral markers of collagen denaturation and hydration in human cortical bone tissue are affected by radiation sterilization and high cycle fatigue damage, J Mech Behav Biomed Mater. 75 (2017) 314–321. doi:10.1016/j.jmbbm.2017.07.016. [PubMed: 28772165]

[63]. Nyman JS, Uppuganti S, Unal M, Leverant CJ, Adabala S, Granke M, et al., Manipulating the Amount and Structure of the Organic Matrix Affects the Water Compartments of Human Cortical Bone, JBMR Plus. 3 (2019) e10135. doi:10.1002/jbm4.10135. [PubMed: 31346566]

[64]. Mandair GS, Morris MD, Contributions of Raman spectroscopy to the understanding of bone strength, Bonekey Rep. 4 (2015) 620–8. doi:10.1038/bonekey.2014.115. [PubMed: 25628882]

[65]. McNerny EMB, Gong B, Morris MD, Kohn DH, Bone Fracture Toughness and Strength Correlate With Collagen Cross-Link Maturity in a DoseControlled Lathyrism Mouse Model, J. Bone Miner. Res 30 (2015) 446–455. doi:10.1002/jbmr.2356.

[66]. Granke M, Does MD, Nyman JS, The Role of Water Compartments in the Material Properties of Cortical Bone, 97 (2015) 292–307. doi:10.1007/s00223-015-9977-5.

[67]. Schriefer JL, Robling AG, Warden SJ, Fournier AJ, Mason JJ, Turner CH, A comparison of mechanical properties derived from multiple skeletal sites in mice, 38 (2005) 467–475. doi: 10.1016/j.jbiomech.2004.04.020.

[68]. Abar O, Dharmar S, Tang SY, The effect of aminoguanidine (AG) and pyridoxamine (PM) on ageing human cortical bone, Bone Joint Res. 7 (2018) 105–110. doi: 10.1302/2046-3758.71.BJR-2017-0135.R1. [PubMed: 29363521]

[69]. Gallant MA, Brown DM, Hammond M, Wallace JM, Du J, Deymier-Black AC, et al., Bone cell-independent benefits of raloxifene on the skeleton: a novel mechanism for improving bone material properties, 61 (2014) 191–200. doi:10.1016/j.bone.2014.01.009.

[70]. Alliston T, Biological regulation of bone quality, Curr Osteoporos Rep. 12 (2014) 366–375. doi: 10.1007/s11914-014-0213-4. [PubMed: 24894149]

Highlights

- Toughness and fracture toughness of cortical bone decrease with advanced age in female and male BALB/c mice.
- Accompanying the loss in material properties are several age-related changes in the extracellular matrix such as lower bound water fraction.
- Sex-related differences include higher cortical thickness and bending strength with age (females) but lower cortical thickness and no strength difference (males).

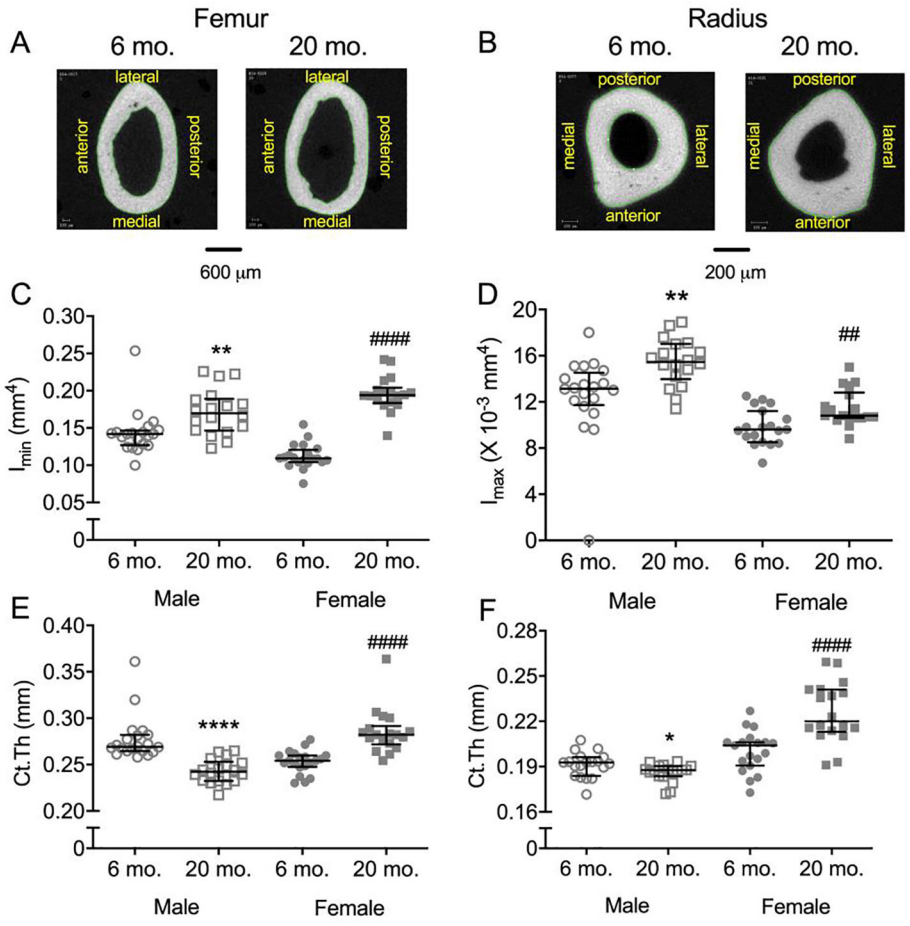

Figure 1:

Structural characteristics of the mid-diaphysis with representative μCT images of male femurs (A) and radii (B). The minimum principal second moment of area (I_{min}) of the femur (C) and the maximum principal second moment of area (I_{max}) of the radius (D) was higher for old mice than for young adult mice, irrespective of sex. Cortical thickness (Ct.Th) of the femur (E) and radius (F) however was higher for old females but lower for old males compared to young adult mice. **p<0.01 and ****p<0.0001 within male. ###p<0.001 and ####p<0.0001 within female.

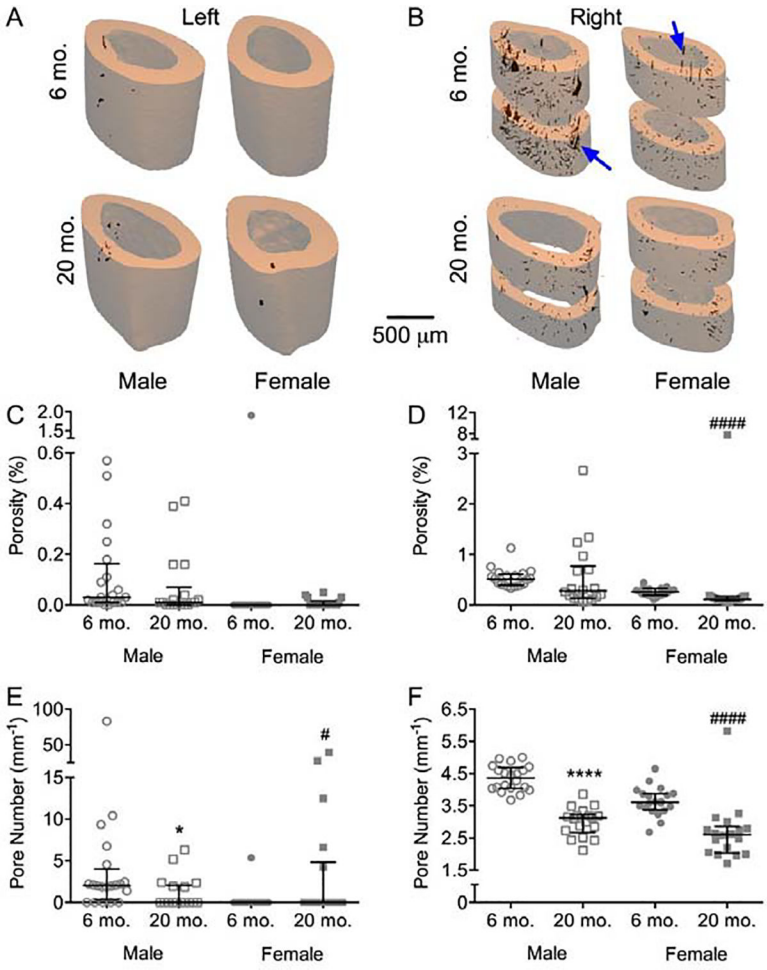

Figure 2:

Cortical porosity from μCT evaluations of the left and right femurs. Representative three-dimensional renderings from the intact (A) and notched femurs (B) show that the higher resolution of the latter partially resolved what appear to be vascular channels. By 12 μm (C) or 6 μm (D) voxel size, porosity either did not vary between the age groups or was lower with age. Pore number for both the left (E) and right (F) imaging was lower in the diaphysis from old mice than from young adult mice. . *$p<0.05$ and ****$p<0.0001$ within male. #$p<0.05$ and ####$p<0.0001$ within female.

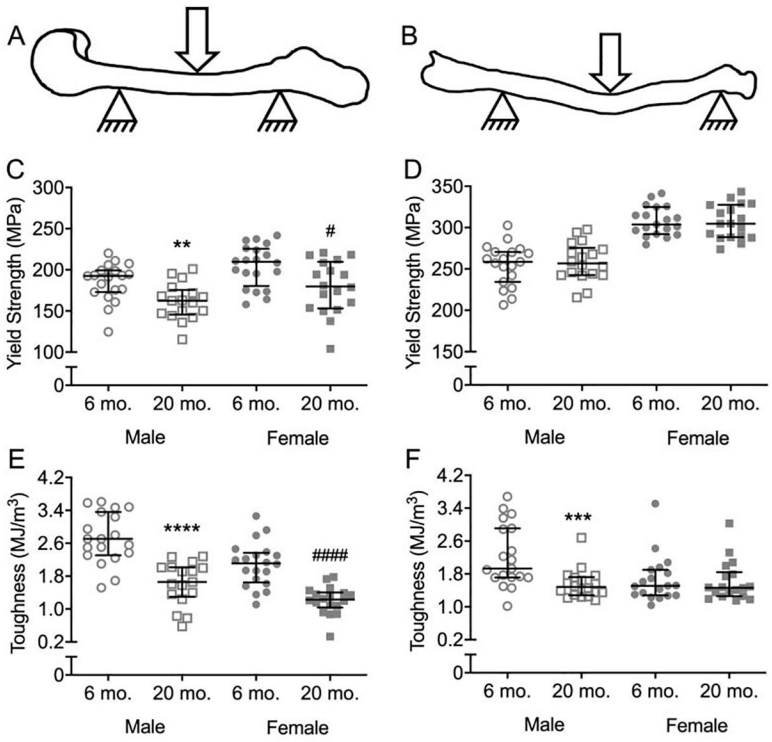

Figure 3:

Estimated material properties of cortical bone. Drawings of the three-point bending tests are shown for both the femur (A) and radius (B). Yield stress of the cortical bone was lower for old mice than for the young adult mice when the femur (C), but not the radius (D), was tested. While toughness was lower for both the old male and female mice, compared to respective young adult mice, when the femur was tested (E), it was only lower for old than for young adult males when the radius was tested (F). **p<0.01, ***p<0.001 and ****p<0.0001 within male. #p<0.05 and ####p<0.0001 within female.

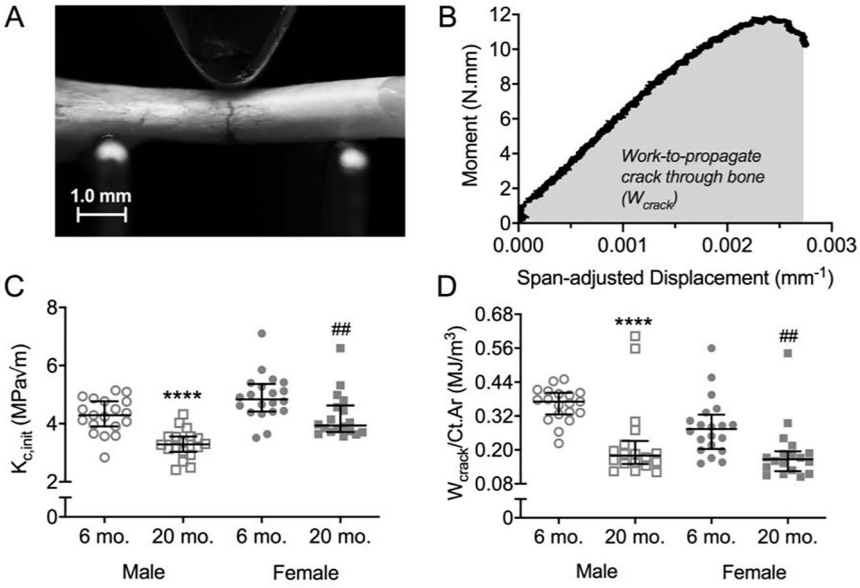

Figure 4:

Crack resistance of the femoral cortex. In fracture toughness tests, a crack is propagated by loading a femur mid-shaft with a micro-notch on the tension side of bending (A). The stress intensity to initiate the crack was estimated from the yield moment, and the work during crack growth (W_{crack}) per bone cross-sectional area (Ct.Ar) was estimated from the area under the moment vs. span-adjusted displacement curve (B). $K_{c,init}$ (C) and W_{crack}/Ct.Ar (D) were lower for old than young adult mice in both sexes. ***p<0.001 and ****p<0.0001 within male. ##p<0.01 and ####p<0.0001 within female.

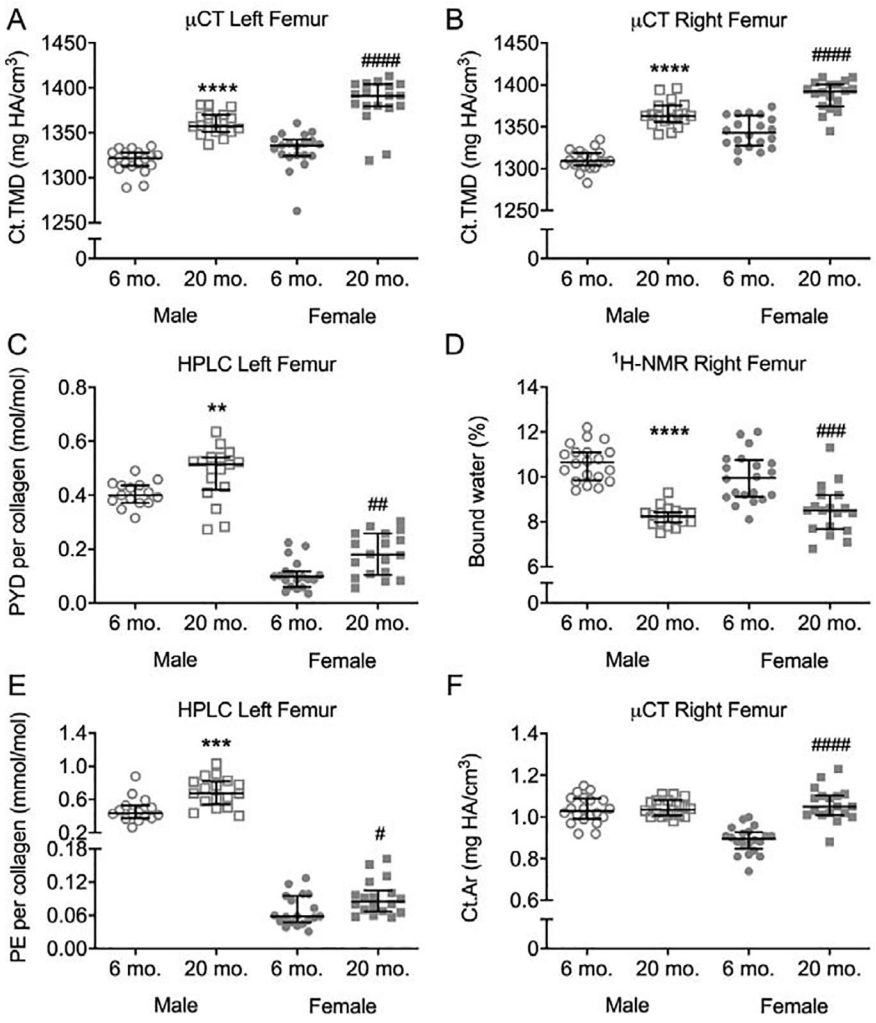

Figure 5:

Age-related changes in bone matrix characteristics of BALB/c femoral diaphysis. Ct.TMD of the intact femoral mid-shaft (A) and notched femoral mid-shaft (B) was higher at 20-mo. than at 6-mo. Mature enzymatic (PYD) collagen crosslink was higher (C), while bound water was lower (D) with advanced age. A non-enzymatic collagen crosslink (PE) was also higher for aged mice than young adult mice (E). Cross-sectional area of the mid-shaft was only higher with age for female mice (F). 6-mo mice are represented by circles and 20-mo. mice are represented by squares. **p<0.01, ***p<0.001, ****p<0.0001 within male. #p<0.05, ##p<0.01, ###p<0.001 and ####p<0.0001 within female.

Bone. Author manuscript; available in PMC 2021 January 01.

Table 1.

Body weight and selected properties from caliper measurements, μCT evaluations, and three-point bending tests of the femur and radius.

		Male							**Female**						
		6-mo. (n ≥ 19)			**20-mo. (n ≥ 17)**				**6-mo. (n ≥ 19)**			**20-mo. (n = 18)**			
Property	**Unit**	**median**	**(25th,**	**75th)**	**median**	**(25th,**	**75th)**	**p-value**	**median**	**(25th,**	**75th)**	**median**	**(25th,**	**75th)**	**p-value**
Global									*Global*						
Body mass	g	31.9	(31.7,	33.3)	30.5	(30.0,	31.6)	**0.001**	25.9	(25.0,	26.8)	26.8	(25.3,	29.5)	0.131
Femur									*Femur*						
Length	mm	14.7	(14.5,	15.0)	14.9	(14.7,	15.1)	0.254	14.8	(14.5,	15.1)	14.8	(14.7,	15.0)	0.578
Ct.Ar[a]	mm^2	1.10	(1.08,	1.14)	1.08	(1.03,	1.14)	0.373	0.93	(0.90,	0.97)	1.10	(1.09,	1.15)	**<0.0001**
Tt.Ar[b]	mm^2	1.81	(1.71,	1.87)	2.07	(1.92,	2.15)	**<0.0001**	1.51	(1.47,	1.57)	1.85	(1.83,	1.93)	**<0.0001**
Modulus	GPa	9.1	(7.2,	10.1)	10.6	(7.2,	11.6)	0.060	11.0	(10.2,	11.5)	11.3	(10.1,	11.9)	0.734
PY tough[c]	N/mm^2	1.89	(1.3,	2.25)	1.04	(0.79,	1.29)	**<0.0001**	1.00	(0.77,	1.21)	0.29	(0.12,	0.67)	**<0.0001**
PYD[d]	mm^{-1}	0.0438	(0.0342,	0.0513)	0.0238	(0.0180,	0.0269)	**<0.0001**	0.0342	(0.0255,	0.0388)	0.0148	(0.0107,	0.0206)	**<0.0001**
Ultimate moment	Nmm	52.5	(50.3,	54.8)	55.4	(47.9,	58.3)	0.401	43.1	(40.5,	46.0)	60.1	(53.9,	61.3)	**<0.0001**
Yield moment	Nmm	41.1	(39.2,	45.4)	44.6	(37.9,	47.8)	0.808	39.0	(37.1,	42.6)	49.4	(44.4,	56.6)	**<0.0001**
Rigidity	Nmm^2	1161	(1015,	1368)	1624	(1457,	1871)	**<0.0001**	1173	(1098,	1417)	2151	(1950,	2269)	**<0.0001**
Work-to-fracture[e]	N	2.92	(2.66,	3.42)	1.74	(1.54,	2.16)	**<0.0001**	1.81	(1.68,	2.07)	1.40	(1.09,	1.57)	**0.0003**
Radius									*Radius*						
Ct.TMD	mgHA/cm^3	1164	(1157,	1172)	1216	(1204,	1225)	**<0.0001**	1175	(1168,	1189)	1243	(1236,	1249)	**<0.0001**
Ct.Ar[a]	mm^2	0.297	(0.291,	0.304)	0.310	(0.302,	0.319)	**0.029**	0.268	(0.260,	0.283)	0.304	(0.296,	0.316)	**<0.0001**
Tt.Ar[b]	mm^2	0.371	(0.349,	0.381)	0.406	(0.386,	0.423)	**<0.0001**	0.327	(0.309,	0.341)	0.345	(0.342,	0.362)	**0.003**
Modulus	GPa	13.0	(11.1,	13.9)	13.7	(12.8,	14.8)	0.073	16.9	(15.8,	17.4)	16.5	(15.7,	17.3)	0.753
PY tough[c]	N/mm^2	0.991	(0.816,	2.080)	0.606	(0.502,	0.788)	**0.0003**	0.371	(0.308,	0.711)	0.348	(0.302,	0.675)	0.875
Py-d[d]	mm^{-1}	0.0447	(0.0367,	0.1059)	0.0204	(0.0181,	0.0274)	**0.0001**	0.0151	(0.0108,	0.0348)	0.0132	(0.0121,	0.0269)	0.922
Ultimate moment	Nmm	8.55	(8.1,	9.26)	9.85	(9.39,	10.60)	**<0.0001**	8.24	(8.03,	8.57)	9.38	(8.98,	9.68)	**0.001**
Yield moment	Nmm	8.24	(7.67,	9.00)	9.39	(8.93,	10.00)	**0.0002**	8.20	(7.91,	8.47)	9.29	(8.95,	9.68)	**0.0004**

		Male							Female						
		6-mo. (n ≥ 19)			20-mo. (n ≥ 17)				6-mo. (n ≥ 19)			20-mo. (n = 18)			
Property	**Unit**	**median**	**(25th,**	**75th)**	**median**	**(25th,**	**75th)**	**p-value**	**median**	**(25th,**	**75th)**	**median**	**(25th,**	**75th)**	**p-value**
Rigidity	Nmm^2	161	(150,	185)	215	(194,	221)	**<0.0001**	160	(152,	170)	189	(177,	203)	**0.001**
Work-to-fracture[e]	N	0.570	(0.512,	0.839)	0.462	(0.402,	0.480)	**0.001**	0.421	(0.338,	0.480)	0.432	(0.396,	0.539)	0.196

[a] Bone cross-sectional area of the cortex was the average of mid-shaft slices after segmentation.

[b] Total cross-sectional area of the mid-shaft was the average of areas defined by periosteal contours.

[c] Post-yield toughness is the energy dissipated after bone yields.

[d] Post-yield displacement is the deflection from yield point to the fracture point and adjusted for differences in span.

[e] Since the span of the three-point bending fixture varied, displacement (d) was adjusted ($12 \times d / span^2$) and work-to-fracture was the area under the moment vs. adjusted-displacement curve.

Table 2.

Selected properties from Raman spectroscopy analysis of the anterior surface of the tibia (proximal half).

		Male							**Female**						
		6-mo. (n = 11)			**20-mo. (n = 11)**				**6-mo. (n ≥ 19)**			**20-mo. (n = 18)**			
Property	**Unit**	**median**	**(25th,**	**75th)**	**median**	**(25th,**	**75th)**	**p-value**	**median**	**(25th,**	**75th)**	**median**	**(25th,**	**75th)**	**p-value**
Left tibia									***Right tibia***[a]						
v_1PO_4/Amide I[a]	–	33.0	(31.6,	34.4)	38.1	(33.4,	42.0)	**0.034**	42.1	(35.2,	45.7)	52.3	(46.6,	55.7)	**<0.0001**
v_1PO_4/Proline[a]	–	21.1	(19.7,	25.0)	27.0	(26.0,	29.9)	**0.010**	30.3	(16.0,	37.3)	43.8	(28.3,	56.4)	**0.003**
v_1PO_4/Amide III[a]	–	8.98	(6.99,	9.99)	12.44	(10.62,	14.22)	**0.007**	7.71	(6.21,	9.22)	9.90	(8.91,	11.99)	**0.001**
v_1PO_4/CH_2[a]	–	8.78	(7.19,	9.42)	12.13	(9.69,	13.04)	**0.005**	7.92	(6.37,	9.37)	10.20	(9.54,	12.15)	**0.0002**
CO_3/v_1PO_4[b]	–	0.146	(0.142,	0.152)	0.157	(0.151,	0.161)	**0.006**	0.141	(0.139,	0.146)	0.151	(0.147,	0.154)	**<0.0001**
Crystallinity[c]	cm	0.0546	(0.0543,	0.0562)	0.0567	(0.0563,	0.0578)	**0.006**	0.0564	(0.0559,	0.0569)	0.0583	(0.0580,	0.0586)	**<0.0001**
I_{1670}/I_{1610}[d]	–	3.62	(3.06,	4.64)	5.04	(3.58,	5.85)	**0.038**	3.90	(3.00,	4.22)	4.61	(4.40,	4.99)	**0.002**
I_{1670}/I_{1640}[d]	–	1.81	(1.71,	1.84)	1.92	(1.88,	1.98)	**0.004**	1.81	(1.76,	1.91)	2.01	(1.86,	2.09)	**0.001**
I_{1670}/I_{1690}[d]	–	2.20	(2.16,	2.43)	2.03	(2.01,	2.09)	**0.0001**	2.04	(1.90,	2.23)	2.00	(1.73,	2.09)	0.096

[a]Each mineral-to-matrix ratio is the peak intensity at ~960 cm^{-1} (phosphate) divided by one of the organic matrix-associated peaks. Four are reported because of their varying degree of sensitivity to matrix organization (fibril orientation).

[b]Carbonate peak at ~1072 cm^{-1} divided by the phosphate peak.

[c]The full-width at half maximum of the phosphate peak. The Amide I sub-peak ratios were directly determined from sub-peak heights – identified by the second derivative spectrum – divided the Amide I peak at ~1667 cm^{-1}.